Journal of Nuclear Materials 605 (2025) 155568



Contents lists available at ScienceDirect

Journal of Nuclear Materials

journal homepage: www.elsevier.com/locate/jnucmat





Inhibition of uranium dissolution in mixed uranium thorium dioxide under geological disposal conditions

Emma Perry McLean [*], Aleksej Popel [1], Ian Farnan

University of Cambridge, Cambridge, CB2 3EQ, United Kingdom

ARTICLE INFO

Keywords:
Uranium dioxide
Geological disposal
Spent nuclear fuel
Disposal MOx
Thorium dioxide
Hydrogen peroxide

ABSTRACT

A safety case supporting the direct disposal of spent mixed oxide (MOx) nuclear fuels in a deep geological repository (DGR), or of plutonium waste processed into a disposal MOx, must consider not only the local redox conditions but also the impact of the additional actinide on the oxidation and subsequent dissolution of the uranium dioxide matrix in the event of container breach. The higher alpha radiation field surrounding plutonium containing fuels increases the production of radiolytic oxidants close to the surface of the fuel and which could enhance the oxidative dissolution of uranium compared to UO_2 fuels. Conversely, doping uranium dioxide with less soluble actinides, has the potential to stabilise the uranium dioxide matrix. Thorium is analogous to plutonium in the latter respect. Model MOx fuel pellets, of lower radioactivity, containing uranium and thorium dioxide have been fabricated and their dissolution studied under conditions relevant to geological disposal. The environment of a deep repository with a clay host rock is simulated by the imposition of anoxic conditions and use of dearated synthetic Callovian Oxfordian ground waters, containing 0.5 mmol.L^{-1} hydrogencarbonate ions, doped with 0.1 mmol.L^{-1} hydrogen peroxide. The uranium release and peroxide consumption over time are compared in static batch experiments with UO_2, ThO_2 and $U_{0.75}Th_{0.25}O_2$ pellets and to blank experiments.

In experiments with UO_2 and $U_{0.75}Th_{0.25}O_2$ pellets, dissolution is independent of hydrogen peroxide concentration, rather the dissolution is controlled by the conduction of holes. The homogeneous doping of uranium dioxide with 25% thorium dioxide has reduced the normalised uranium release by at least a factor of five when compared with the dissolution of undoped uranium dioxide pellets. Hole conduction appears more limiting in the case of mixed uranium thorium oxide pellets due to Th(IV). The results presented here support the proposition that despite the increased radioactivity of MOx fuel, disposal of MOx would not have a solubility greater than UOx (uranium oxide) spent fuel under these conditions.

Laboratory simulation of radiolytic production has been improved by development of a method by which a syringe pump continuously adds ground waters doped with hydrogen peroxide in batch systems. This overcomes the time limitations of conventional batch dissolution with peroxide that decomposes within a period of several days. Uranium dissolution of mixed uranium thorium dioxide pellets is similar in the static batch experiments with and without continuous additions of hydrogen peroxide. In this regime where uranium dissolution is independent of hydrogen peroxide concentration, the dissolution yield is not a useful parameter to compare between different experimental methods.

1. Introduction

Geological disposal of spent nuclear fuel is internationally recognised as the safest long term disposal solution for nuclear fuel waste. Deep geological repositories are designed with a multi-barrier approach, to prevent radioactive release to the environment by limiting contact between the fuel and ground waters for 10,000 years. By this point significant amounts of the radioactivity will have decayed. Most of the radioactive inventory is contained within the uranium dioxide matrix, which acts as the primary barrier. Callovian Oxfordian groundwaters, typical of the low strength sedimentary rock geology of the French disposal site, have been seen to suppress uranium dissolution [16,26]. Dissolution of uranium dioxide in near-neutral ground waters is slow in the reducing conditions of a disposal facility but can increase due to

* Corresponding author.
E-mail addresses: emma.perry@stfc.ac.uk, ema_p.202@hotmail.com (E. Perry McLean).
[1] Current affiliation: Seaborg technologies, Copenhagen, 2200, Denmark.

https://doi.org/10.1016/j.jnucmat.2024.155568
Received 14 March 2024; Received in revised form 10 December 2024; Accepted 12 December 2024
Available online 16 December 2024
0022-3115/© 2024 The Authors. Published by Elsevier B.V. This is an open access article under the CC BY license (http://creativecommons.org/licenses/by/4.0/).

the oxidising nature of radiolytic species produced close to the fuel, of which hydrogen peroxide is the most dominant [28].

The dissolution of uranium dioxide by hydrogen peroxide can be studied as a corrosion process with hydrogen peroxide reduced at a cathodic site on the surface of the fuel [28]. Electron holes are then conducted through the fuel surface to the anode where either uranium is oxidised or the hydrogen peroxide is, described as a catalytic decomposition of hydrogen peroxide. In hydrogencarbonate solutions, the oxidisation of uranium is likely to lead to dissolution and so the uranium oxidation rate is approximated as the uranium dissolution rate.

Mixed oxide (MOx) fuels consist of uranium and plutonium dioxide. Spent MOx fuels are typically five times as radioactive as uranium based fuels of similar burn up [15]. The safety case for MOx disposal therefore has to account for a higher rate of radiolytic production. MOx dissolution is of particular interest in the United Kingdom as a disposal waste form for contaminated plutonium, now unsuitable for reprocessing [20]. Mixed thorium uranium dioxide fuels are of interest in their own right and a plan for their disposal would be required before they could used commercially [30,12].

Dissolution experiments with MOx fuels have found low dissolution yields, below 1% suggesting that plutonium in the uranium dioxide matrix could stabilise the uranium against dissolution [26,25,16]. This is reasonable since the plutonium oxide is more durable than uranium dioxide in aqueous solution. In these experiments the radiolytic species are produced in situ by the high activity plutonium. Since the production rates are much lower for undoped uranium dioxide, it has not been possible to make an experiment directly comparing the dissolution of plutonium doped and undoped uranium dioxide. How the plutonium could slow dissolution is not fully understood but the lack of plutonium dissolution was used to suggest a plutonium rich phase could passivate the surface [15].

In this work uranium thorium dioxide is used as a model of uranium plutonium dioxide. Thorium in thorium dioxide remains in Th(IV) oxidation state and is used as an analogue of Pu(IV). The ionic radii of 8-coordinated four-valent actinides are close enough to allow full solid solution across the compositional range obeying Vegard's law. Like PuO_2, ThO_2 has with a low, negative solubility product in near neutral pH [23,24]. This model fuel has been produced with a homogeneous distribution of 25% thorium, to model the plutonium content of the plutonium starting material in MOx fuels produced using the MIMAS process [33]. $U_{0.75}Th_{0.25}O_2$ pellets were leached in synthetic Callovian Oxfordian groundwaters doped with 0.12 mmol.L^{-1} hydrogen peroxide, at room temperature, in a static batch arrangement. The solutions were sampled throughout 60 days without replenishment. Endmember pellets, UO_2 and ThO_2 were leached in the same conditions. The ability to directly compare to the end member materials is a significant advantage of the model fuel experiments allowing the separation of the dopant effect from many other factors that can influence the dissolution.

However the static batch method does not simulate radiolytic production. In the batch experiment there is an initial concentration of hydrogen peroxide whereas in an experiment with real fuel, there is no initial concentration. Dissolution at longer times is more interesting to the spent fuel community but the length of the static batch experiments are limited by the lifetime of hydrogen peroxide. For example [16] have seen a rate change after 50 days, a potential passivisation effect that might not be accessible in the static batch method. To improve upon the static batch method, **a continuous additions dissolution method** has been developed and applied to study of the mixed uranium thorium oxide pellets. Note that the continuous additions method is not the same as a flow through experiment. There is no outlet flow and the volume is maintained as fairly close to constant by the periodic sampling.

Table 1
Concentrations in mg.L^{-1} of COx argillite pore water at 25 ^{o}C modelled by [35,10] with the average of 3 samples of the initial synthetic COx ground waters measured by ICP-MS in this study with (error).

	Na^+	Si	Mg^{2+}	K^+
Model	994	5.1	131	40.7
Actual	990(10)	5.6(0.6)	130(10)	38(4)

	Cl^-	Sr^{2+}	Ca^{2+}	SO_4^{2-}	HCO_3^{2-}
Model	1453	18.4	1412	341	148
Actual	1400(140)	17(2)	340(30)		

2. Materials and methods

2.1. Pellet sample fabrication

A solution of 1 mol.L^{-1} uranyl nitrate hexahydrate and 0.33 mol.L^{-1} thorium nitrate hexahydrate was reduced with 5% H_2/Ar in the presence of a platinum foil for 16 hours inside an argon atmosphere glovebox. The powders and pellets remained in this glovebox until characterisation. Oxalate powders were then made using a simplified co-precipitation method adapted from [1] wherein the nitrate solution was slowly added in a dropwise manner to 1 mol.L^{-1} oxalic acid at room temperature. The resulting oxalates were filtered out and rinsed several times with dearated 1% oxalic acid. These powders underwent a thermal decomposition under argon in alumina crucibles at 800 ^{o}C, to form oxide powders and then reduced under 5% H_2/Ar at 800 ^{o}C. Complete oxalate decomposition is expected to occur above 700 ^{o}C [8]. The oxide powders were ground using an agate pestle and mortar before pressing into 5 mm diameter pellets at 150 MPa for one minute. The pellets were sintered on tungsten foil lined alumina crucibles in a furnace inside the argon atmosphere glovebox for 16 hours dwell time at 1600 ^{o}C with a heating rate up to 25 ^{o}C/min. Pellets were stored under an argon atmosphere and reduced under 5% H_2/Ar for 3 hours at 1000 ^{o}C before dissolution experiments. The method to fabricate end member pellets was very similar without the need to reduce the nitrate hexahydrate solutions initially.

2.2. Dissolution experimental method

For the static batch experiments, new sterile 125 ml Naglene polypropylene bottles were filled 10% volume with deionised water and shaken for 30 seconds. This was repeated 3 times per vessel. For the experiments with continuous additions, 60 ml PTFE savilex jars were submerged in fresh nitric acid for 1 hr, 24 hr, 1 hr, 24 hr at 90 ^{o}C and then the process was repeated in deionised water at 90 ^{o}C. Between solution changes the jars were filled with 10 ml deionised water and shaken for 30 seconds. The same vessels were used for the preleach, the dissolution study and an acid rinse at the end. The vessels and solutions were kept under argon atmosphere throughout.

Pellets were produced inside of an argon atmosphere glovebox and were reduced in 5% H_2/N_2 at 1000 ^{o}C for 2.5 hours prior to dissolution without air exposure. The pellets were then preleached in hydrogencarbonate solutions to remove any oxidised uranium at the surface of the pellet. Each preleach involved a 24 hour dwell in 50 ml of dearated 10 mmol.L^{-1} sodium hydrogencarbonate solution, without hydrogen peroxide, at room temperature. Each pellet and the empty vessels for the blank experiments were subjected to the preleach procedure twice. After the preleach, the pellets and empty vessels were rinsed with dearated deionised waters.

The leachant in these dissolution studies, synthetic COx solutions, were made fresh with initial ion concentrations listed in Table 1 and verified by ICP-MS. The concentrations of ground water ions remained within 1 std of the initial solution throughout the experiment. The

ground water solutions were dearated and the oxygen content was confirmed to be less than 0.05 mg.L^{-1} using a colorimetric test kit (chemetrics R-7501).

In the static batch experiments the leachant was initially doped with 0.12 mmol.L^{-1} hydrogen peroxide and its consumption was observed over time using UV/vis spectroscopy. The bottles in the static batch experiments were opened, in the argon glovebox, for solution changes and sampling. Samples were taken without replenishment such that the volume began at 100 ml and ended around 60 ml. The surface area to volume ratio was on the order of 0.1 m^{-1}. Ion concentrations were measured by ICP-MS, hydrogen peroxide concentrations by UV/vis spectroscopy and pH was measured ex-situ by a Metler Toledo five easy FE20 pH bench meter inside the argon atmosphere. Experiments are performed in duplicate with deionised water blanks and synthetic COx water blanks.

In experiments with continuous additions, the experiments began with synthetic COx ground water and ground water solutions doped with $5.8 \cdot 10^{-4}$ mol.L^{-1} hydrogen peroxide was added at a flow rate of 6.5 nL.s^{-1} by a syringe pump through a PTFE tube directed through a small hole in the lid. The vessels were sampled through a second small hole in the lid that was closed off between sampling. The initial volume was 50 ml and remained about 50 ± 3 ml throughout since the sampling volumes were chosen to equal the volume of the continuous additions. Before the 5 ml syringes emptied, the additions were paused, the syringe solutions were sampled, emptied and refilled with stock dearated ground waters with hydrogen peroxide freshly added. The 6% hydrogen peroxide solutions were bought fresh and stored in a chiller at about 5 ^{o}C throughout the experiment. Three experiments with mixed uranium thorium oxide pellets with continuous additions were run in parallel to three blank experiments without pellets. This simulation is equivalent to a dose rate of 10^{5} Gy.hr^{-1} from alpha emitting 3.8 mm diameter, 0.6 mm thick pellets in water [32,31]. Experiments were performed in triplicate with synthetic COx water blanks.

At the end of the study, an additional sample for ICP-MS was passed through a wetted 0.45 μm syringe filter. The oxidation reduction potential was measured in situ with a micro combination probe from Metler Toledo in the presence of the pellet. These measurements were directly correlated to the hydrogen peroxide concentration. Pellets were rinsed in deionised water, patted dry with a wiper and left in the glovebox for further SEM/EDX and Raman analysis. Additional samples were collected for total alkalinity determination of the hydrogencarbonate concentrations. Finally, the vessels were washed out by filling with 50 ml nitric acid solution (2 mol.L^{-1}) for 24 hours twice to dissolve precipitated phases.

2.3. Additional methods detail

Samples collected for **Inductively coupled plasma mass spectroscopy** were acidified and immediately diluted with concentrated nitric acid by a factor of 10, to 1% nitric acid, to reduce the matrix effects of the groundwater ions. The intensities were calibrated using uranium and thorium doped synthetic COx groundwater and SPS-SW2 standard solution. The uranium thorium composition of the mixed oxide was determined by an ICP-MS study of the oxalate powder dissolved in nitric acid.

The UV/visible spectroscopy method for determining hydrogen peroxide concentrations using N,N-dimethyl-p-phenylenediamine dye was developed by [2]. A flame micro spectrometer was set up with fibre optic connectors into the argon atmosphere glovebox so that samples could be tested soon after sampling without any interference from air oxidation. Samples were diluted to within the detectable range of $1 \cdot 10^{-6}$ to $1.5 \cdot 10^{-5}$ mmol.L^{-1}, they were buffered by sodium phosphate monobasic and sodium phosphate dibasic and the oxidation reaction was catalysed by peroxidase. The absorbance was converted to a hydrogen peroxide concentration using a calibration curve produced using diluted groundwater solutions.

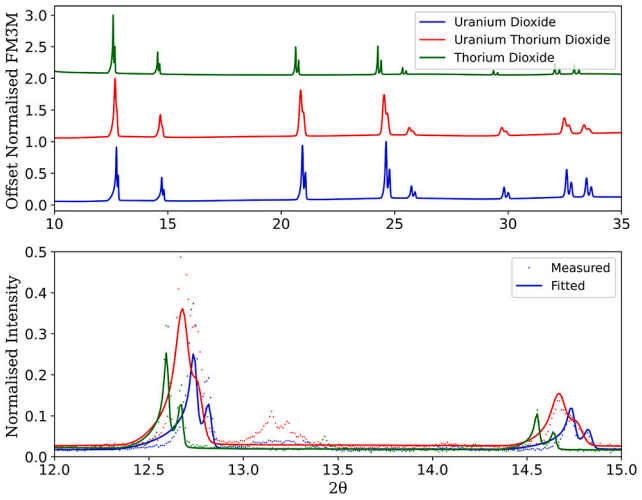


Fig. 1. Molybdenum sourced X-Ray diffraction spectra (with kα1 and kα2 Xrays causing peak splitting) with the calculated fits for $Fm\bar{3}m$. Bottom: Comparing the 12-15 degrees 2θ region measured data (dotted points) with the refined fit (solid line) for $Fm\bar{3}m$ and corundum standard. UO_2 (blue) goodness of fit 3.1, rwp 13.3. $UThO_2$ (red) goodness of fit 6.7, rwp 32.7. ThO_2 (green) goodness of fit 2.6, rwp 15.7. (For interpretation of the colours in the figure(s), the reader is referred to the web version of this article.)

SEM and EDX data were collected on a thermo scientific quanta-650F SEM. Porosity and grain sizes determined from a representative 3,500 μm^2 back-scattering electron data using ImageJ software.

Geometric surface area was calculated from measurements of the diameter and height using calipers. These measurements were used with a measurement of the mass to calculate the **density**. To compare density between different materials the density is converted to a percentage of the theoretical density.

Raman Spectroscopy was performed on a Horiba LabRAM using a 632 nm laser with 180 grooves/mm diffraction grating. The hole size was set to 400 and scans were 20 seconds long with three accumulations. Raman spectroscopy was performed through a polythene bag, sealed under argon atmosphere but the samples had previously be exposed to air during XRD.

The total alkalinity can be determined by titration with acid using the equilibrium hydrogencarbonate ions in solution as the pH only drops once all of the hydrogencarbonate has reacted.

$$H_2CO_3 \rightleftharpoons H^+ + HCO_3^- \rightleftharpoons 2H^+ + CO_3^{2-} \quad (1)$$

At a pH of 8.3 hydrogencarbonate is the dominant carbon species and there would be little contribution to the alkalinity from hydroxyl groups. hydrogencarbonate ions in solution equilibrate with carbon dioxide. Without a carbon dioxide over pressure, hydrogencarbonate concentrations will decrease over time.

XRD (Xray diffraction) was carried out on a molybdenum sourced Bruker D8 advance diffractometer with a Lynx-Eve XET position sensitive detector. A corundum standard was positioned next to the pellet on a zero background plate.

2.4. Pellet sample characterisations

One pellet in each batch was reserved for characterisation.

Refinement of the XRD pattern, as presented in Fig. 1 indicates a crystalline face centred cubic structure, as typical for uranium dioxide. Uranium thorium dioxides are known to follow Vegard's law [3,13,14] and so refinement of the lattice parameter, as listed in Table 2, can indicate the actinide composition. However oxidation can alter the lattice parameters and since XRD is performed under air atmosphere, this determination was not found to be reliable. Additional peaks fitting to a

Table 2
Summary of the key characteristics of the pellets before leaching.

	UO_2	$U_{0.75}Th_{0.25}O_2$	ThO_2
XRD lattice param (Å)	5.4917 ± 0.0001	5.5057 ± 0.0002	5.5958 ± 0.0001
Average geometrical density ($g.cm^{-3}$)	10.6 ± 0.1	10.4 ± 0.1	7.9 ± 0.7
Average geometrical density as a % of the theoretical density	96 ± 10%	97 ± 10%	79 ± 8%
Porosity from SEM	0.5%	6%	3%
Maximum grain size (μm) by SEM	17	13	17
Average grain size (μm) by SEM	5.2	4.5	4.9
Geometric surface area (mm^2)			
S.a.	33	36	29
S.b.	31	30	30
CA.a	-	29	-
CA.b	-	31	-
Mass (mg)			
S.a.	80	55	46
S.b.	66	54	46
CA.a	-	62	-
CA.b	-	74	-

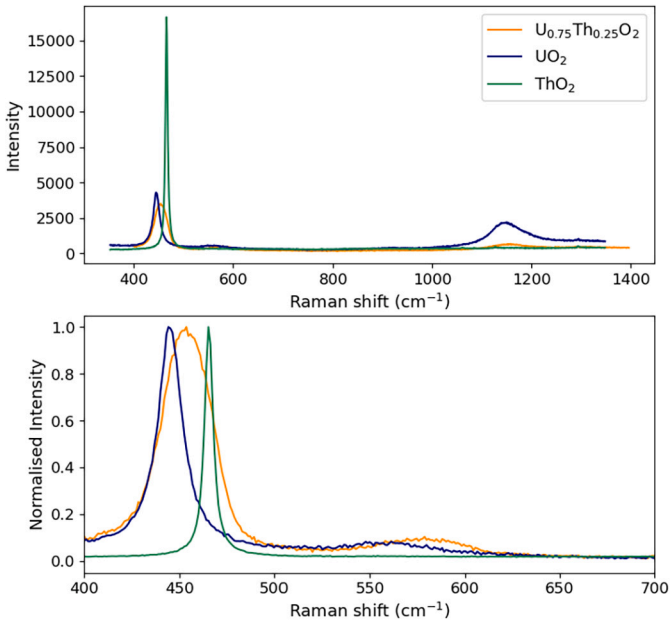


Fig. 2. Raman spectroscopy using a 632 nm excitation, of the mixed uranium thorium dioxide and endmembers.

structureless P121/c1 phase were found to appear over time but could not be identified without high resolution XRD.

Similarly, the position the T_{2g} peak at 465 cm^{-1} indicates the actinide composition [27] but it is likely that oxidation in the characterisation stages have also caused a deviation from theoretical values, which is more pronounced for the more easily oxidised uranium dioxide pellets. The position of Raman spectroscopy at 11 evenly spaced points, 10 μm apart found that the actinide fractions varied less than 10% indicating again that the actinides were homogeneously distributed [16]. The longitudinal peaks at 575 and 1150 cm^{-1} arise from defects, the later is the most sensitive to oxygen vacancies [27]. The peak at 575 cm^{-1} is a convolution of 3 defect peaks, with 550 cm^{-1} associated with grain boundaries, 575 cm^{-1} to defects (causing this shift in the peak seen more for mixed oxide pellets) and oxygen vacancy and 630 cm^{-1} to oxygen clustering [34]. These are not present in thorium dioxide samples as seen in Fig. 2.

Therefore the actinide composition of the mixed uranium thorium oxide sample was determined from ICP-MS of the oxalate precursor

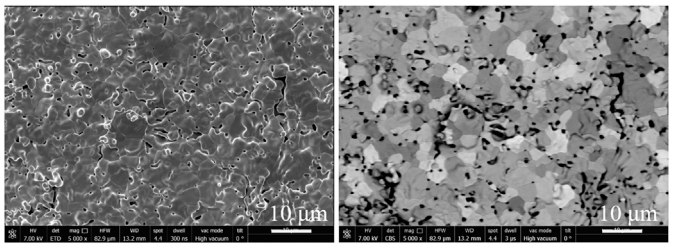


Fig. 3. Left; Secondary electron, Right; Back-scattered electron, images collected on ETD and CBS detectors with a 7.5 kV, 4.5 spot size beam under high vacuum at 5,000 times magnification of the unpolished mixed uranium thorium dioxide pellet.

as the most direct measurement. Oxalate powders were digested in 2 $mol.L^{-1}$ nitric acid and the solution was sampled and diluted for ICP-MS immediately.

SEM images of the mixed uranium thorium oxide pellet, are presented in Fig. 3. For mixed oxides, the first stage in sintering is diffusion of uranium into thorium dioxide regions to make the distribution homogeneous. This additional step delayed the sintering of mixed oxide pellets such that they have more porosity and smaller grains than the end member pellets [7]. The addition of the grinding stage to the fabrication method was seen to increase the density of the end member pellets such that closed porosity could be achieved. The high density of the pellets is indicative of a homogeneous distribution of actinides since the uranium diffusion into thorium rich regions is the first stage of sintering and closing of pores occurs later [6]. The maximum grain sizes listed in Table 2 for all pellets, are on a similar scale to the plutonium rich agglomerates in MIMAS fuel of 20 μm [33].

No uranium concentrations were found above the detection limit, 30 ppt, 1.3 $\times 10^{-7}$ $mol.L^{-1}$, for any preleaching solutions in this work suggesting that uranium was not preoxidised.

3. Theory and calculation

The dissolution of uranium dioxide by hydrogen peroxide can be studied as a corrosion process with hydrogen peroxide reduced at a cathodic site on the surface of the fuel [28]. Electron holes are then conducted through the fuel surface to the anode where either uranium is oxidised or the hydrogen peroxide is, described as a catalytic decomposition of hydrogen peroxide. In hydrogencarbonate solutions, the oxidisation of uranium is likely to lead to dissolution and so the uranium oxidation rate is approximated as the uranium dissolution rate.

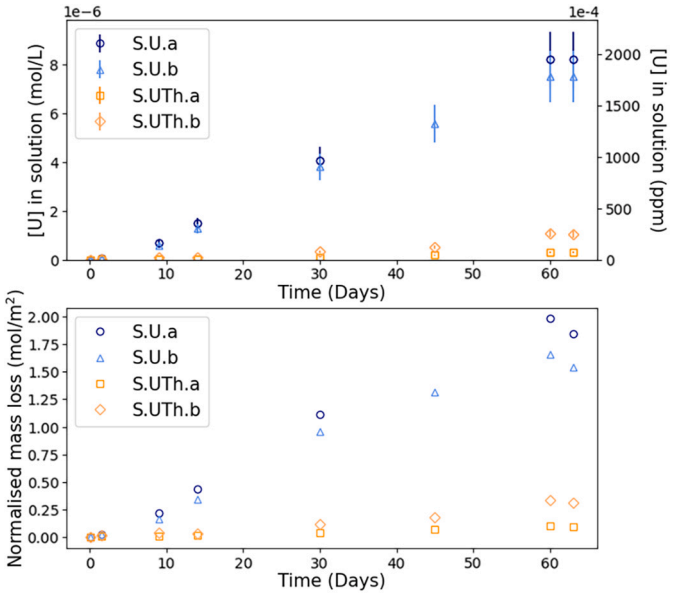


Fig. 4. The concentrations of uranium found in solution in static batch experiments with mixed uranium thorium dioxide and uranium dioxide. Top: Concentration in solution. Right: moles of uranium dissolution per surface area of uranium. a and b are repeats of the same experiment performed at the same time.

The d**issolution yield** is a term used to describe the percentage of cathodic reactions leading to dissolution

$$Dissolution\ Yield(\%) = 100.\frac{[U]}{[H_2O_2]_{consumed}} \tag{2}$$

This parameter is independent of the surface area or, more pertinently, the density of reactive sites. The dissolution yield parameter is a useful parameter in computational models and to compare experiments where the dissolution is dependent on the hydrogen peroxide concentration.

4. Results

4.1. Static batch experiments

Fig. 4 presents the uranium dissolved into solution over time in static batch experiments with uranium containing pellets. Uranium dissolution is reduced by a factor of five or more by doping uranium dioxide with 25% thorium. The normalised mass loss is calculated to account for the lower uranium fraction, x, or surface area, SA, by

$$m_N = \frac{[U]_{solution} \times volume}{x \times SA}. \tag{3}$$

This is plotted in Fig. 4 and one can see that the dissolution is still reduced in the mixed oxide case. The gradient of a linear line of best fit through the normalised mass loss gives the dissolution rate listed in Table 3.

No thorium was detectable in any solution above the limit of 0.3 ppt, 1.3 nmol.L^{-1}. This is a similar result to that of [23] where thorium dioxide dissolution was only detectable using a radioisotope approach. No thorium enrichment of the mixed oxide surface could be detected after leaching by EDS or Raman, however this is to be expected since the altered thickness calculated in Table 3 are much smaller than the approximate 1 μm penetration depth of these techniques.

By comparison the leached uranium dioxide pellet is presented in Fig. 5. Small dots (dark in BSE, light in SE) appear across the surface after leaching in Fig. 5 for uranium dioxide pellets, indicating pitting of the surface. While dissolution is known to take place at grain boundaries in acidic solution, it has not been verified at higher pHs [9]. Grain boundary outlines have a higher contrast after leaching, indicating etching. No altered phase could be distinguished other than the salt dendrites, particles on the surface, that probably formed on the surface during drying.

Table 3
The rates of uranium dissolution into solution calculated from a linear line of best fit through normalised mass loss data. Altered thickness assumes the dissolution was uniform across the pellet surface. S. denotes static batch experiments, CA. denotes experiments with continuous additions. a and b are repeat dissolution experiments performed in parallel of with pellets produced at the same time.

	Normalised rate (μmol. m^{-2}.day^{-1})	± 1 std.	Altered Thickness (μm)	± 1 std.
S.U.a	290	40	0.4	0.1
S.U.b	270	20	0.3	0.1
S.U0.75Th0.25.a	16	1	0.020	0.006
S.U0.75Th0.25.b	57	2	0.05	0.01
CA.U0.75Th0.25.a	2.4	0.2	0.04	0.01
CA.U0.75Th0.25.b	18	1	0.14	0.04
CA.U0.75Th0.25.c	7.1	0.7	0.07	0.02

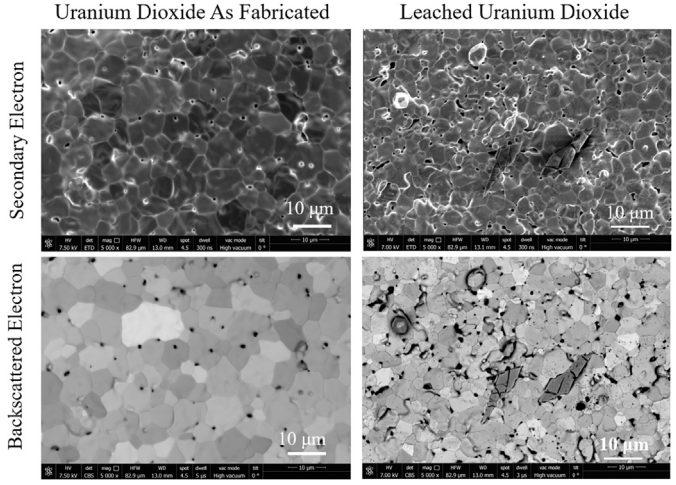


Fig. 5. SE and BSE images of uranium dioxide pellet reserved for characterisation and another after dissolution.

Fig. 6 shows the hydrogen peroxide concentration in solution over time in experiments with uranium containing pellets and their associated blanks. In the blank experiments, in peroxide doped synthetic COx ground waters without pellets, the peroxide concentration was stable over the period of the experiment. The presence of a uranium containing pellet causes the hydrogen peroxide concentration to decrease over time. The amount of consumed hydrogen peroxide is calculated as the difference between the result and the average of the two blank groundwater experiments. The difference in the hydrogen peroxide consumption is not discernible between uranium dioxide and mixed uranium thorium dioxide pellets. In static batch experiments with end member thorium dioxide pellets, no hydrogen peroxide consumption was distinguishable from the blank experiments.

4.2. Batch experiment with continuous additions of hydrogen peroxide

In these experiments the peroxide concentrations were expected to increase over time due to continuous additions of hydrogen peroxide as shown by the calculated line in Fig. 7. The jump between days 8 and 12 was caused by a stronger hydrogen peroxide concentration in the syringe solution. Considering firstly just the blank experiments, one can see two distinct behaviours, one where the concentration increases as calculated

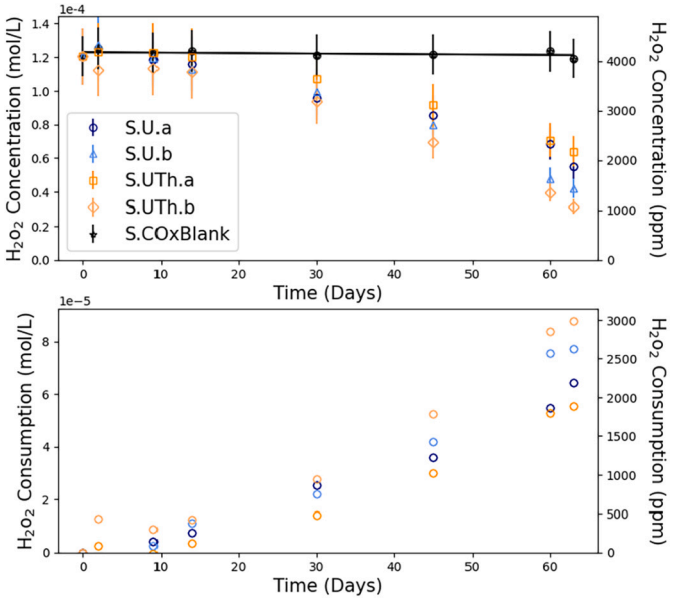


Fig. 6. Top: The hydrogen peroxide concentrations over time in static dissolution experiments as calculated from UV/visible absorbance. The average of the two synthetic COx groundwater's is plotted with a linear line of best fit to guide the eye. Bottom: The consumption of hydrogen peroxide as calculated by subtraction from the blank concentration. a and b are repeats of the same experiment performed at the same time.

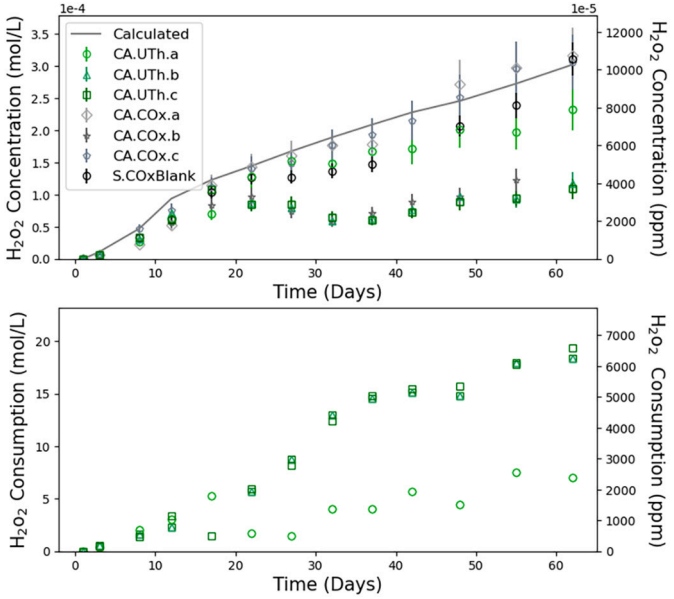


Fig. 7. Top: Hydrogen peroxide concentrations over time in batch experiments with continuous additions of hydrogen peroxide with (UTh) and without (COx) pellets. Calculated line is the hydrogen peroxide concentration without hydrogen peroxide consumption based on additions of known volumes of known hydrogen peroxide concentration. Bottom: Consumed hydrogen peroxide is relative to the calculated concentration. a,b and c are repeats of the same experiment performed at the same time.

and one in which an equilibrium hydrogen peroxide concentration was established about 0.1 mmol.L^{-1} after 20 days. The cause of the later behaviour is unknown but two of the experiments with pellets are effected in a similar way. There were no measurable differences in COx water ion concentrations (which were steady over time), total alkalinity or pH of the leachant, vessel cleaning routine. No precipitated phases were found by analysis of the washout. The hydrogen peroxide concentrations of the syringe solutions were within experimental error initially and at the refill points so the cause is something inside of the experimental vessel itself. At the end of the 60 day study, the oxygen content was found to be under 0.05 mg.L^{-1} in the experiments without background decomposition of hydrogen peroxide. In the blank experiment with continuous additions and background decomposition, the solution oxygen content was above the threshold. In the experiments with background decomposition and pellets, the oxygen content was below the threshold, presumably having been used in oxidation of pellets.

Since the oxygen produced in background decomposition interacts with the pellets it is appropriate to consider the total consumption in the calculation of the dissolution yield. The total consumption of hydrogen peroxide is then the difference between the calculated increase in hydrogen peroxide concentration caused by the continuous additions and that measured as shown in Fig. 7.

In each experiment with continuous additions, uranium dissolution slows after around 35 days, as presented in Fig. 8. This occurs at different concentrations for each experiment so does not appear to be a saturation effect. As in the static batch experiments, no colloids larger than 0.45 μm were found by ICP-MS of filtered solutions.

In the static batch experiments hydrogencarbonate concentrations determined by total alkalinity measurements (as described in additional methods detail) were seen to decrease from 42 to 35 mg.L^{-1}. This drop is due to the absence of a carbon dioxide over pressure but not dissimilar from the concentrations detected in solutions after 150 days with a carbon dioxide over pressure [15]. In experiments with continuous additions they decreased to 25 mg.L^{-1}. Although the flow was very slow, it is possible that the flow disturbed the carbon in the solution increased the equilibrium rate constant. Alternatively, the enhanced reduction in alkalinity could be due to the increased sampling frequency which

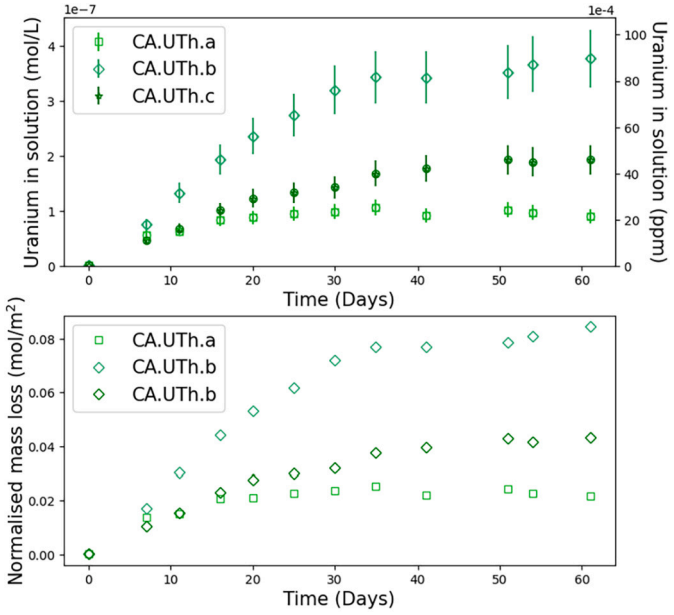


Fig. 8. Uranium dissolved into solution in batch experiments of $U_{0.75}Th_{0.25}O_2$ pellets with continuous additions. a,b and c are repeats of the same experiment performed at the same time.

would disturb the gas in the vessel headspace (10 ml in the continuous additions experiments, 25-65 ml in the static batch experiments). The reduction in hydrogencarbonate concentrations in these experiments with continuous additions of hydrogen peroxide could be the cause of the slowing of the uranium dissolution rate. The pH was consistently around 8.3 ± 0.2 throughout all experiments.

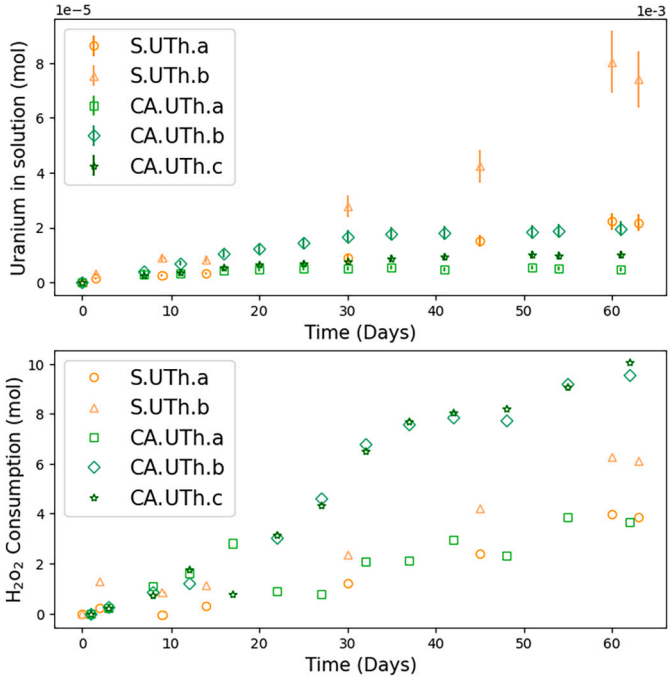


Fig. 9. Cumulative moles of uranium dissolved into solution, with (CA) and without (S) continuous additions of hydrogen peroxide.

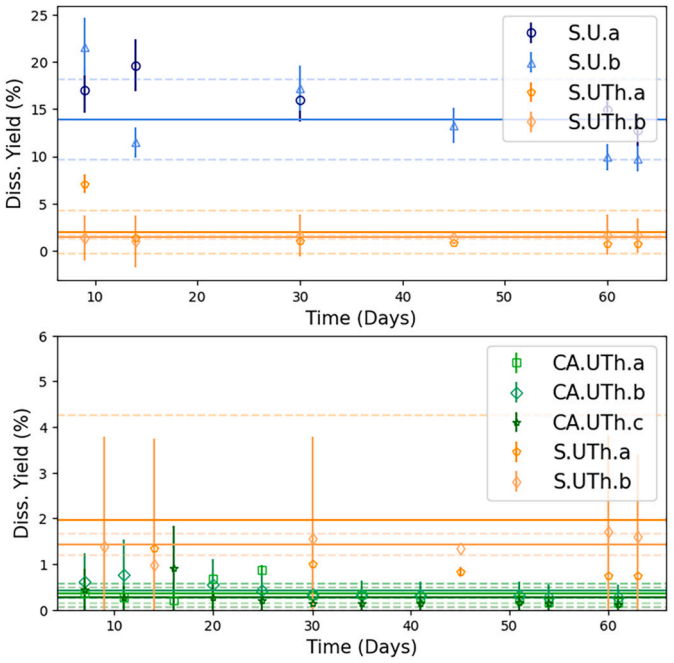


Fig. 10. The dissolution yields calculated at each sampling point plotted with the mean dissolution yield (solid line) and ± 1 std. (dotty line).

4.3. Comparison of static experiments to those with continuous additions

Fig. 9 compares uranium dissolution and peroxide consumption for the same type of mixed oxide pellets in both leaching arrangements. The gradient of the linear section is used to calculated the normalised dissolution rate presented in Table 3. The normalised dissolution rates for mixed uranium thorium pellets are similar between static batch experiments and experiments with the continuous additions method. There is only one experiment with continuous additions without background disproportionation of hydrogen peroxide, CA.UTh.a, which can really be compared to the static batch experiments.

4.4. Dissolution yield

The dissolution yields is plotted in Fig. 10 as a means of comparing between pellets and experimental set ups. The repeat experiments fall within experimental error of each other in static batch experiments but different pellets have a distinctly different dissolution yield. The variation of experimental set up cause a distinct change in dissolution yield.

5. Discussion

5.1. Dissolution of uranium dioxide pellets

The concentrations of hydrogen peroxide used in static batch experiments are quite low in this work, 0.1 mmol.L^{-1}, as compared to other works [4,21,17] where the concentrations are 0.2 - 2 mmol.L^{-1}. In this work peroxide decomposes at a slower rate and so the early day behaviour can be better studied.

In this case it can be seen that uranium dissolution begins immediately and with a constant rate. Hydrogen peroxide consumption rate tends to increase as seen by the more curved profile in Fig. 6. Evidence suggests that catalytic decomposition occurs at mixed valence sites [19]. Whilst uranium is oxidised immediately and removed from the surface at a constant rate throughout the 60 days, the mixed valence sites for catalytic decomposition do not form until around day 15. The two processes are disconnected. Then to further support this, even though the peroxide concentrations are decreasing, the dissolution rate is constant, suggesting that the concentration of hydrogen peroxide is not the limiting factor in these experiments.

5.2. Effect of thorium doping

It has been suggested that uranium release from the mixed uranium thorium dioxide is inhibited by a thin layer of re-precipitated thorium hydroxide at the surface [11]. Endmember thorium dioxide pellets in this work did not have any measurable catalytic effect on the decomposition of hydrogen peroxide. If a thorium rich layer formed at the surface of mixed oxide pellets then the consumption of hydrogen peroxide should have reduced over time, which it did not. However a surface sensitive technique like X-ray photo-electron spectroscopy (XPS) would be required to know for certain.

The hypothesis is that the uranium dissolution is reduced by the presence of thorium in the UO_2 lattices inhibiting electron hole conduction. This explanation is consistent with this work while the formation of a thorium-rich protective surface layer is not. This is supported by the XPS evidence presented by [11] and cyclic voltametry presented by [5]. By XPS it has been possible to observe bulk sample oxidation in uranium dioxide in contrast to uranium thorium dioxide samples where oxidation is limited to the surface. Much higher potentials were required to oxidise thorium doped uranium dioxide than undoped samples.

Mixed oxide pellets catalyse hydrogen peroxide decomposition in much the same way as end member uranium dioxide. In mixed oxide pellet experiments, the uranium is oxidising to form the mixed valance catalytic sites but not dissolving which again separates the two processes.

In examining the behaviour of $(U,Ce)O_2$ compositions in the presence of H_2O_2, Montaigne et al. show that the presence of Ce(IV) can inhibit the dissolution of U, but only when homogeneously substituted [22]. This further supports the important role of the substitutuent in mixed uranium oxides in preventing oxidation where Montaigne et al. have carefully evidenced the Ce(IV) oxidation state to avoid uncertainties about the Ce(III)/Ce(IV) couple.

5.3. Dissolution yield

There is a variation in uranium dissolution between repeat experiments with mixed oxide pellets presented in Fig. 4 and 8. This difference is likely to be due to the number of reactive sites given the similarity between the dissolution yield calculated for repeat experiments as presented in Fig. 10. The dissolution yield is independent of surface area and this is a benefit of the parameter.

An issue with the dissolution yield parameter arises when comparing between the static batch and continuous additions experiments. In these experiments, hydrogen peroxide concentration is not the limiting factor in dissolution and an increase in the peroxide consumed, the quotient, simply decreases the yield.

Additionally if the catalytic decomposition and dissolution really are two separate processes as previously discussed then the premise of the favoured anodic reaction is invalid and removes the theoretical basis of a dissolution yield.

The concept of the dissolution yield being a ratio of anodic reactions is further invalidated by the effects of background hydrogen peroxide decomposition. In the experiments with continuous additions where background disproportionation occurred, uranium still dissolved. [29] present evidence that the oxidation rate of uranium by oxygen is 200 times slower than by hydrogen peroxide, due to the strength of the oxygen bond. On the other hand [18] find oxygen to have a higher relative impact in the dissolution of SIMFUELs. In this case, where dissolution is limited by hole mobility, the difference between hydrogen peroxide and oxygen could make little difference. In the definition of anodic reactions leading to dissolution, background disproportionation should be subtracted. Since the oxygen produced in background disproportionation can cause dissolution the total consumption, both on the anodic site and away from it, should be used to calculate the dissolution yield. Note that in literature experiments where radiolytic oxidants are produced in situ there is no measure of the background disproportionation and the total consumption is used also.

Many groups including [15,4], also observe a background disproportionation particularly in solutions containing ground water ions. Although steps can be taken to reduce this background disproportionation, by blocking sunlight, maintaining a rigorous cleaning procedure, neutral pH and low peroxide concentrations, the background disproportionation can occur somewhat erratically in laboratory experiments. In this work, it has been possible to run blank experiments in parallel. These blank experiments have exactly the same conditions so that background effects can be separated. When determining mechanisms, this is an advantage over experiments with plutonium where the radiolytic oxidants are produced in situ at a rate that cannot be measured directly and is therefore calculated.

Further work should develop the method of the batch experiments with continuous additions of hydrogen peroxide to simulate more realistic radiolytic production for longer timescales. The method should be adapted to maintain sufficient hydrogencarbonate concentrations.

Future experiments are easily adapted to lower production rates. As compared to calculations presented by [15], this is an order of magnitude higher than what would be expected of MOx fuels after 50 years of interim storage and 3 orders of magnitude higher than the expected dose rates when breach of containment is predicted to occur.

6. Conclusion

Assuming a similar insulating effect of plutonium doping as compared to thorium on the uranium dioxide conduction band, these results support the disposal of MOx in a geological disposal facility. MOx fuels are likely to produce radiolytic oxidants at five times the rate of uranium based fuels but this work has found homogeneous thorium doping to reduce the dissolution rate by over five times. This brings the uranium release from mixed oxide fuels within the bounds of a uranium-based fuel safety case.

The dissolution yield has been found to have limited usefulness in scenarios when hydrogen peroxide is in excess and when uranium dissolution and hydrogen peroxide decomposition are separated in time. Instead, normalised dissolution rates can be compared between experiments with continuous additions to static batch experiments and with literature results. The normalised dissolution rate for $U_{0.75}Th_{0.25}O_2$ pellets was similar between experiments with continuous additions to static batch experiments.

CRediT authorship contribution statement

Emma Perry McLean: Writing – original draft, Visualization, Methodology, Investigation, Formal analysis, Data curation. **Aleksej Popel:** Writing – review & editing, Resources, Methodology, Conceptualization. **Ian Farnan:** Writing – review & editing, Supervision, Resources, Investigation, Funding acquisition, Conceptualization.

Declaration of competing interest

The authors declare the following financial interests/personal relationships which may be considered as potential competing interests: Emma Therese Perry McLean reports financial support was provided by European Commission, Modern Spent Fuel Dissolution and Chemistry in Failed Container Conditions (DisCo) grant number: 755443. If there are other authors, they declare that they have no known competing financial interests or personal relationships that could have appeared to influence the work reported in this paper.

Acknowledgements

Dr Jason Day for ICP-MS data collection.
Dr Giulio Lampronti for XRD and SEM training.
Dr Jeremie Asseline for Raman spectroscopy training.
Dr Oscar Branson for UV/visible spectroscopy.
Christopher Parish for furnace part manufacture.

Data availability

Data will be made available on request.

References

[1] Y. Altaş, M. Eral, H. Tel, Preparation of homogeneous (Th0.8U0.2)O2 pellets via co-precipitation of (Th,U) (C2O4)2 · nH2O powders, J. Nucl. Mater. 249 (1997) 46–51, https://doi.org/10.1016/S0022-3115(97)00185-2.
[2] H. Bader, V. Sturzenegger, J. Hoigne, Photometric method for the determination of low concentrations of hydrogen peroxide by the peroxidase catalyzed oxidation of n, n-diethyl-p-phenylenediamine (dpd), Water Res. 22 (1988) 1109–1115.
[3] L. Balice, D. Bouëxière, M. Cologna, A. Cambriani, J.F. Vigier, E. De Bona, G.D. Sorarù, C. Kübel, O. Walter, K. Popa, Nano and micro u1-xthxo2 solid solutions: from powders to pellets, J. Nucl. Mater. 498 (2018) 307–313.
[4] A. Barreiro Fidalgo, Y. Kumagai, M. Jonsson, The role of surface-bound hydroxyl radicals in the reaction between H 2 O 2 and UO 2, J. Coord. Chem. 71 (2018) 1799–1807, https://doi.org/10.1080/00958972.2018.1466287.
[5] P. Cakir, R. Eloirdi, F. Huber, R.J. Konings, T. Gouder, Thorium effect on the oxidation of uranium: Photoelectron spectroscopy (XPS/UPS) and cyclic voltammetry (CV) investigation on (U 1x Th x)O 2 (x0 to 1) thin films, Appl. Surf. Sci. 393 (2017) 204–211, https://doi.org/10.1016/j.apsusc.2016.10.010.
[6] L. Claparede, N. Clavier, N. Dacheux, A. Mesbah, J. Martinez, S. Szenknect, P. Moisy, Multiparametric dissolution of thorium-cerium dioxide solid solutions, Inorg. Chem. 50 (2011) 11702–11714, https://doi.org/10.1021/ic201699t.
[7] L. Claparede, N. Clavier, A. Mesbah, F. Tocino, S. Szenknect, J. Ravaux, N. Dacheux, Impact of the cationic homogeneity on Th 0.5 U 0.5 O 2 densification and chemical durability, J. Nucl. Mater. 514 (2019) 368–379, https://doi.org/10.1016/j.jnucmat.2018.12.009.
[8] N. Clavier, N. Hingant, M. Rivenet, S. Dobbade, N. Dacheux, N. Barŕe, F. Abraham, X-ray diffraction and μ-Raman investigation of the monoclinic- orthorhombic phase transition in Th 1 - x U x (C 2 O 4) 2 · 2H 2 O solid solutions, Inorg. Chem. 49 (2010) 1921–1931, https://doi.org/10.1021/ic902343r.

[9] C.L. Corkhill, E. Myllykyla, D.J. Bailey, S.M. Thornber, J. Qi, P. Maldonado, M.C. Stennett, A. Hamilton, N.C. Hyatt, Contribution of energetically reactive surface features to the dissolution of ceo2 and tho2 analogues for spent nuclear fuel microstructures, ACS Appl. Mater. Interfaces 6 (2014) 12279–12289.
[10] E.C. Gaucher, C. Tournassat, F. Pearson, P. Blanc, C. Crouzet, C. Lerouge, S. Altmann, A robust model for pore-water chemistry of clayrock, Geochim. Cosmochim. Acta 73 (2009) 6470–6487.
[11] G. Heisbourg, S. Hubert, N. Dacheux, J. Purans, Kinetic and thermodynamic studies of the dissolution of thoria-urania solid solutions, J. Nucl. Mater. 335 (2004) 5–13, https://doi.org/10.1016/j.jnucmat.2004.05.017.
[12] J.S. Herring, P.E. MacDonald, K.D. Weaver, C. Kullberg, Low cost, proliferation resistant, uranium–thorium dioxide fuels for light water reactors, Nucl. Eng. Des. 203 (2001) 65–85.
[13] S. Hubert, J. Purans, G. Heisbourg, P. Moisy, N. Dacheux, Local structure of actinide dioxide solid solutions th1-x u x o2 and th1-x pu x o2, Inorg. Chem. 45 (2006) 3887–3894.
[14] M. Kanno, S. Kokubo, H. Furuya, Preparation of thorium-uranium mixed oxide pellets, J. Nucl. Sci. Technol. 19 (1982) 956–958.
[15] V. Kerleguer, Apport de l'étude de matériaux modèles U1-xPuxO2 à la compréhension des mécanismes d'altération des combustibles UOx et MOx en stockage géologique, Ph.D. thesis, Université Paris Sciences et Lettres, 2020.
[16] V. Kerleguer, C. Jégou, L. De Windt, V. Broudic, G. Jouan, S. Miro, F. Tocino, C. Martin, The mechanisms of alteration of a homogeneous U0.73Pu0.27O2 MOx fuel under alpha radiolysis of water, J. Nucl. Mater. 529 (2020), https://doi.org/10.1016/j.jnucmat.2019.151920.
[17] Y. Kumagai, A. Barreiro Fidalgo, M. Jonsson, Impact of stoichiometry on the mechanism and kinetics of oxidative dissolution of UO2 induced by H2O2 and γ-irradiation, J. Phys. Chem. C 123 (2019) 9919–9925, https://doi.org/10.1021/acs.jpcc.9b00862.
[18] C.M. Lousada, M. Trummer, M. Jonsson, Reactivity of H2O2 towards different UO 2-based materials: the relative impact of radiolysis products revisited, J. Nucl. Mater. 434 (2013) 434–439, https://doi.org/10.1016/j.jnucmat.2011.06.003.
[19] C.M. Lousada, M. Yang, K. Nilsson, M. Jonsson, Catalytic decomposition of hydrogen peroxide on transition metal and lanthanide oxides, J. Mol. Catal. A, Chem. 379 (2013) 178–184, https://doi.org/10.1016/j.molcata.2013.08.017.
[20] A. Macfarlane, F. von Hippel, J. Kang, R. Nelson, Plutonium disposal, the third way, Bull. At. Sci. 57 (2001) 53–57.
[21] A.C. Maier, Dynamics of Spent Nuclear Fuel Dissolution: Impact of Catalysis, Matrix Composition and Time Evolution, Ph.D. thesis. School of Engineering Sciences in Chemistry, Biotechnology and Health, 2019, https://doi.org/10.1017/CBO9781107415324.004, arXiv:1011.1669v3.
[22] T. Montaigne, S. Szenknect, V. Broudic, P.H. Imbert, F. Tocino, C. Martin, F. Miserque, C. Jégou, N. Dacheux, Oxidative dissolution of (u, ce) o2 materials in aqueous solutions containing h2o2, npj Mater. Degrad. 7 (2023) 34.
[23] E. Myllykylä, Investigation of ThO2 as a structural analogue for spent nuclear fuel dissolution under repository conditions, Ph.D. thesis, Faculty of Science of the University of Helsinki, 2017.
[24] V. Neck, M. Altmaier, R. Müller, A. Bauer, T. Fanghänel, J.I. Kim, Solubility of crystalline thorium dioxide, Radiochim. Acta 91 (2003) 253–262, https://doi.org/10.1524/ract.91.5.253.20306.
[25] M. Odorowski, C. Jegou, L. De Windt, V. Broudic, G. Jouan, S. Peuget, C. Martin, Effect of metallic iron on the oxidative dissolution of UO2 doped with a radioactive alpha emitter in synthetic Callovian-Oxfordian groundwater, Geochim. Cosmochim. Acta 219 (2017) 1–21, https://doi.org/10.1016/j.gca.2017.08.043.
[26] M. Odorowski, C. Jégou, L. De Windt, V. Broudic, S. Peuget, M. Magnin, M. Tribet, C. Martin, Oxidative dissolution of unirradiated Mimas MOX fuel (U/Pu oxides) in carbonated water under oxic and anoxic conditions, J. Nucl. Mater. 468 (2016) 17–25, https://doi.org/10.1016/j.jnucmat.2015.09.059.
[27] R. Rao, R.K. Bhagat, N.P. Salke, A. Kumar, Raman spectroscopic investigation of thorium dioxide-uranium dioxide (ThO2-UO2) fuel materials, Appl. Spectrosc. 68 (2014) 44–48, https://doi.org/10.1366/13-07172.
[28] D. Shoesmith, Fuel corrosion processes under waste disposal conditions, J. Nucl. Mater. 282 (2000) 1–31, https://doi.org/10.1016/S0022-3115(00)00392-5.
[29] D.W. Shoesmith, S. Sunder, M.G. Bailey, G.J. Wallace, F. Stanchell, Anodic oxidation of UO_2, IV. X-ray photoelectron spectroscopic and electrochemical studies of film growth in carbonate-containing solutions, Appl. Surface Sci. 20 (1984) 39–57.
[30] G.P. Smith, J.C. Cunnane, S.W. Spetz, M.S. Kazimi, M.J. Driscoll, A. Solomon, L.F.P.V. Swam, S. Tulenko, E.J. Lahoda, Advanced proliferation resistant, lower cost, uranium-thorium dioxide fuels for light water reactor project, in: Thorium Fuel Utilization: Options and Trends, 2002, IAEA-TECDOC-1319, 99–103.
[31] S. Sunder, Calculation of radiation dose rates in a water layer in contact with used candu uo2 fuel, Nucl. Technol. 122 (1998) 211–221.
[32] S. Sunder, N.H. Miller, XPS and XRD studies of (Th,U)O2 fuel corrosion in water, J. Nucl. Mater. 279 (2000) 118–126, https://doi.org/10.1016/S0022-3115(99)00242-1.
[33] Z. Talip, S. Peuget, M. Magnin, L. Berardo, C. Valot, R. Vauchy, C. Jégou, Raman microspectroscopic studies of unirradiated homogeneous ($U_{0.76}Pu_{0.24}$)O_{2+x}): the effects of Pu content, non-stoichiometry, self-radiation damage and secondary phases, J. Raman Spectrosc. 48 (2017) 765–772, https://doi.org/10.1002/jrs.5092.
[34] B.T. Tan, A.J. Popel, R.J. Wilbraham, J. Day, G.I. Lampronti, C. Boxall, I. Farnan, Surface and electrochemical controls on uo2 dissolution under anoxic conditions, J. Nucl. Mater. 520 (2019) 41–55.
[35] C. Tournassat, P. Blanc, E. Gaucher, Estimation de la composition de l'eau porale du callovo-oxfordien à 50, 70, 80 et 90 c, Rapport final, BRGM report/RP-56171-FR, BRGM, Orléans, France, 2008.